

Multiphonon Raman Scattering from Individual Single-Walled Carbon Nanotubes

Feng Wang,¹ Weitao Liu,¹ Yang Wu,² Matthew Y. Sfeir,³ Limin Huang,⁴ James Hone,⁵
Stephen O'Brien,⁴ Louis E. Brus,³ Tony F. Heinz,² and Y. Ron Shen¹

¹*Department of Physics, University of California at Berkeley, Berkeley, California 94720, USA,
and Materials Science Division, Lawrence Berkeley National Laboratory, Berkeley, California 94720, USA*

²*Departments of Physics and Electrical Engineering, Columbia University, New York, New York 10027, USA*

³*Department of Chemistry, Columbia University, New York, New York 10027, USA*

⁴*Department of Applied Physics and Applied Mathematics, Columbia University, New York, New York 10027, USA*

⁵*Department of Mechanical Engineering, Columbia University, New York, New York 10027, USA*

(Received 25 June 2006; published 23 January 2007)

Combinations of up to 6 zone-edge and zone-center optical phonons are observed in the Raman spectra of individual single-walled carbon nanotubes (SWNTs). These multiphonon Raman modes exhibit distinct signatures of the one-dimensional nature of SWNTs and provide information on the phonon structure, exciton-phonon coupling, and excitonic transitions in nanotubes.

DOI: [10.1103/PhysRevLett.98.047402](https://doi.org/10.1103/PhysRevLett.98.047402)

PACS numbers: 78.67.Ch, 73.22.-f, 78.30.Na, 78.35.+c

Raman scattering has been increasingly employed to characterize lower-dimensional materials, such as nanostructures, that have electronic and phonon properties significantly different from the bulk. Such studies have revealed new features of zero-dimensional nanoparticles [1–3], one-dimensional (1D) carbon nanotubes [4–9], and two-dimensional (2D) quantum wells [10,11]. For a better understanding of the phonon structure and electron-phonon coupling of lower-dimensional materials, one would like to examine not only one-phonon but also multiphonon Raman scattering. Multiphonon Raman scattering is readily detectable in bulk semiconductors when excited near exciton resonances [12–14], but was expected to be weak in nanostructures. Recently, however, it has been observed in ensembles of nanoparticles and carbon nanotubes, and has been used to elucidate exciton-phonon interactions in these materials [1,2,15]. Multiphonon Raman scattering from individual nanoparticles or nanotubes has, to our knowledge, not been reported.

Here we present a Raman study of individual single-walled carbon nanotubes (SWNTs). Clearly resolved and relatively narrow Raman peaks involving up to 6 phonons were observed. They arise from different combinations of the zone-center and pairs of zone-edge optical phonons. In contrast to bulk materials under similar excitation conditions, the successive higher-order modes in the Raman spectra of SWNTs decreased relatively slowly in strength. Raman spectra of different nanotubes and of the same nanotube excited by photons of different energy varied markedly, reflecting the sensitive dependence of the Raman process on both phonon and electronic structure. This behavior underscores the necessity of studying individual nanotubes.

Our study was performed on individual SWNTs suspended across a slit of 40- μm width and 1-mm length. The slit structures were prepared by standard photolithography and wet etching techniques. The SWNTs were grown across the slit by chemical vapor deposition using

a 1-nm-thick Co film as the catalyst and ethanol as the feed gas [16]. The resulting SWNTs were typically separated from one another by $\sim 100\ \mu\text{m}$. The individual SWNTs were characterized by Rayleigh (elastic) light scattering. The Rayleigh scattering spectra, which exhibit resonant enhancement for photon energies matching electronic transitions, provide direct access to the electronic structure and allow us to distinguish between individual nanotubes and nanotube bundles [17,18].

In our Raman measurements, the pump laser beam (at a wavelength of 532 or 473 nm and power of 1 mW) was focused by an objective to $\sim 1\ \mu\text{m}^2$ to illuminate an individual SWNT. The scattered light was collected at an oblique angle by a second objective. The Raman emission was analyzed by a spectrograph equipped with a CCD camera with a resolution of $30\ \text{cm}^{-1}$.

Figure 1 shows Raman spectra of two different individual SWNTs. The data, presented in a log-linear plot, were obtained using 473-nm excitation with both incident and scattered light polarized along the nanotube axis. A wealth of multiphonon Raman modes with frequency shifts greater than $1000\ \text{cm}^{-1}$ can be identified. Rayleigh scattering spectra (analogous to those of Fig. 2) indicated that both of these nanotubes were semiconducting with diameters around 2 nm [17].

The observation of such higher-order multiphonon Raman scattering from an individual SWNT was unexpected: The number of carbon atoms illuminated by the focused laser spot was less than 1% of a monolayer, while observation of Raman scattering from a full molecular monolayer is known to be difficult. Consequently, it was already a surprise when detection of one-phonon Raman scattering from an *individual* SWNT was first reported [19,20]. The unusually strong Raman scattering was attributed to the special nature of the 1D electronic structure of SWNTs. Here we find that the characteristics of this 1D system even permit the detection of *higher-order, multiphonon* Raman modes.

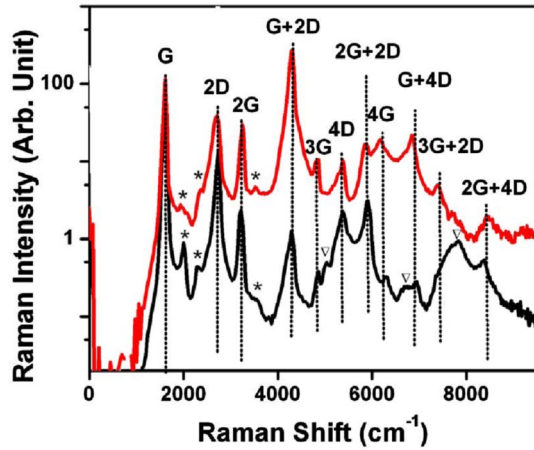


FIG. 1 (color online). Raman spectra of two individual single-walled nanotubes obtained with 473-nm excitation. The spectra are displayed in a log-linear plot. The upper spectrum is displaced for clarity ($\times 10$). Most peaks (indicated by the dashed lines) in the spectra can be assigned to different combinations of the zone-center G mode and even numbers of the zone-boundary D modes (see Table I). There are a few weaker features common to all nanotubes (denoted by $*$) and a few others specific to individual nanotubes (denoted by ∇).

The multiphonon Raman scattering from SWNTs exhibits several distinctive characteristics. (1) The multiphonon Raman spectra display well-defined and relatively narrow features. These features are present in nanotubes of different diameters and chiral indices (Fig. 1), as well as for different photon excitation energies lying well above the fundamental band gap [Figs. 2(a) and 2(b)]. (2) Although the intensity of n -phonon Raman modes generally decreases with increasing value of n , the falloff is slow. This is crucial for the observation of modes involving up to six phonons. (3) The relative intensity of multiphonon modes in different individual nanotubes varies dramatically. There are instances when Raman scattering of certain higher-order modes is actually stronger than scattering by lower-order modes in the same nanotube. In Fig. 2(a), for example, the $2G + 2D$ (peak 7) is stronger than both $2G$ (peak 3) and $G + 2D$ (peak 4).

Before discussing these observations, we first consider identification of the labeled multiphonon Raman lines for the individual SWNTs of Fig. 2. Most of the features originate from combinations of the zone-center G phonons and the zone-boundary D phonons. Only combinations including even number of the D -mode phonons are allowed because of the momentum conservation in the scattering process: D phonons must appear in pairs of approximately opposite wave vector in order to achieve nearly zero overall phonon momentum in the Raman process. Table I lists the measured Raman shifts of these G and $2D$ overtone and combination modes. They agree reasonably well with calculated values for combination modes with frequencies of 1580 and 1340 cm^{-1} for the G and D modes, respectively [4]. We attribute the discrepancies between the calculated

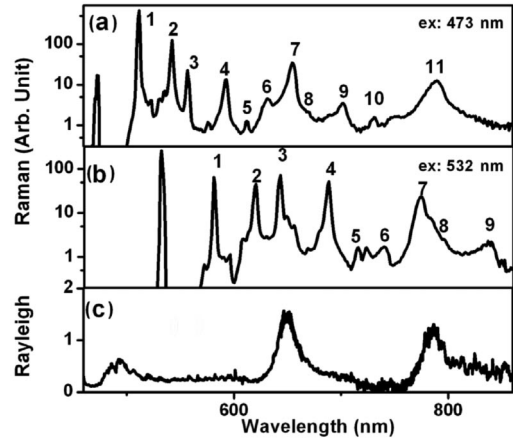


FIG. 2. Comparison of the Raman and Rayleigh excitation spectra for an individual SWNT to illustrate the effect of resonant enhancement in the Raman process. (a) Raman spectrum of the SWNT for laser excitation at a wavelength of 473 nm. The Raman modes are labeled in accordance with Table I. (b) Raman spectrum for laser excitation at 532 nm. (c) Excitation spectrum for Rayleigh (elastic) light scattering from the same nanotube. The two peaks at 650 and 784 nm in the Rayleigh spectrum arise from the E_{44} and E_{33} excitonic transitions of a 2.2 nm semiconducting SWNT [17]. Raman modes with outgoing wavelengths close to these two transitions [peaks 7 and 11 in (a) and peaks 3 and 7 in (b)] exhibit a pronounced resonant enhancement.

and the observed shifts to the phonon dispersion probed by pairs of D phonons that do not originate strictly at the zone boundary. Assignments similar to ours have been given in previous Raman studies of graphite [21] and nanotube bundles [22]. In addition to these principal modes, we observe a set of much weaker Raman features (denoted by $*$ in Fig. 1) that are common to all SWNTs. These weaker features can be explained as combination modes of optical and acoustic phonons near the zone center or/and zone boundaries. For example, the feature at $\sim 1900 \text{ cm}^{-1}$ was assigned in a previous study to a combination mode of a G phonon and an acoustic phonon near the zone center [23]. Further Raman features (denoted by ∇ in Fig. 1) are present only in specific nanotubes. They are likely to be certain weak Raman modes that experience strong resonant enhancement only in the selected nanotube. The broad peak near 8000 cm^{-1} in the lower spectrum of Fig. 1 could also arise from an electronic Raman transition. In the following, we discuss only the strong Raman modes present in all nanotube species that arise from combinations of optical phonons.

Phonons of different wave vectors can participate in multiphonon Raman scattering as long as their total momentum is close to zero. How then are the narrow multiphonon Raman features in nanotubes [observation (1) above] compatible with the significant dispersion known to exist for the phonon bands [4]? Such broadening of multiphonon features is indeed generally seen in bulk materials. In germanium crystals, for example, even

TABLE I. Assignment of the Raman modes from the SWNTs of Fig. 1 in terms of combinations of G - and even number of D -mode phonons. The expected Raman shifts for these modes were calculated assuming frequencies of 1580 and 1360 cm^{-1} for G and D modes, respectively.

Number	Experimental Raman shift (cm^{-1})	Assigned Raman mode	Expected shift (cm^{-1})
1	1600	G	1580
2	2710	$2D$	2680
3	3182	$2G$	3160
4	4296	$G + 2D$	4260
5	4828	$3G$	4740
6	5340	$4D$	5360
7	5891	$2G + 2D$	5840
8	6220	$4G$	6320
9	6904	$G + 4D$	6940
10	7432	$3G + 2D$	7420
11	8400	$2G + 4D$	8520

Raman modes involving just two phonons are extremely broad [24].

To understand the origin of the different behavior in SWNTs, we consider the strength of the matrix element for multiphonon Raman scattering, which can be written approximately as [25]

$$M = \sum_{i_0, \dots, i_n} \left[\frac{\langle f | H_{eR} | i_n \rangle \langle i_0 | H_{eR} | 0 \rangle}{E_{ex} - E_{i_0}} \times \left(\prod_{j=1, \dots, n} \frac{\langle i_j | H_{e-ion} | i_{j-1} \rangle}{E_{ex} - E_{i_j}} \right) \right]. \quad (1)$$

Here H_{eR} denotes the electron-radiation coupling and H_{e-ion} the electron-phonon coupling. E_{ex} is the input photon energy, and i_j describes a state with j phonons and electronic excitation in the i th level. This expression includes two important components: the phonon density of states (DOS) and the electronic resonance factors. In carbon nanotubes, the dispersion of the electronic structure is large, and only states close to the two degenerate zone-boundary points (K and K') can be in resonance at visible photon energies. Transitions between such states, favored by the resonance denominators in Eq. (1), involve optical phonons either near the zone-center Γ point (G mode) or near the zone-boundary K and K' points (D mode). In addition to the propensity for G and D modes from the electronic resonance enhancement, the phonon DOS in 1D is also suitable for multiphonon processes involving such extrema in the phonon dispersion relation. This behavior contrasts to that of 3D materials for which the DOS at such points typically vanishes. Two-phonon Raman scattering at twice the one-phonon (zone-center) Raman energy, for example, is generally absent in 3D materials for this reason [24]. In one dimension, however, the DOS close to the phonon band extrema remains finite. This permits observation of the resonantly enhanced strong multiphonon overtone and combination G - and D -mode Raman features in SWNTs.

Next we consider the strengths of the multiphonon Raman features [observation (2) above] and how they are affected by the 1D nature of SWNTs. We investigate this by comparing the SWNT Raman spectra to that of graphite. Observation of only 5 multiphonon Raman modes— $2D$, $2G$, $2D + G$, $4D$, and $2D + 2G$ —from graphite has been reported [21], as compared to our detection of 10 multiphonon modes from individual SWNTs. The Raman signal in SWNTs decreases with increasing phonon order much more slowly than in graphite. This is evident from Fig. 3, where we show the Raman intensities of different modes (normalized against that of the respective G -mode intensity) for graphite and for several distinct, individual SWNTs. Because the relative strength of successive higher-order Raman modes is proportional to exciton-phonon coupling, our results suggest that isolated individual SWNTs exhibit appreciably stronger exciton-phonon coupling than graphite.

Not only is the decrease of the higher-order Raman intensity slow with increasing mode order for SWNTs, but in specific cases higher-order modes can actually be stronger than the lower-order ones [observation (3) above]. This behavior can be understood as a result of electronic resonances in multiphonon Raman scattering associated with the strongly peaked exciton transitions in SWNTs [26–29]. As seen from Eq. (1), the multiphonon Raman process is resonantly enhanced whenever any intermediate step is near an electronic resonance. In particular, there will be an outgoing resonance when the last step corresponds to emission of the Stokes-shifted photon by an excitonic transition. As shown in Fig. 2 for two different input photon energies, strong enhancement is observed for Raman modes 7 ($2G + 2D$) and 11 ($2G + 4D$) in Fig. 2(a) and modes 3 ($2G$) and 7 ($2G + 2D$) in Fig. 2(b) when the Stokes-shifted photon is resonant with an excitonic transition of the SWNT [Fig. 2(c)]. Such behavior contrasts with that of 3D or 2D materials in which smoothly varying free-carrier band-to-band transitions generally dominate.

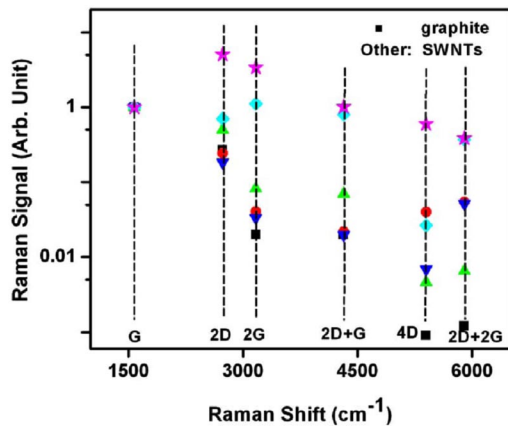


FIG. 3 (color online). Comparison of relative strengths of multiphonon Raman modes observed in graphite [21] (black squares) and in several individual SWNTs (other symbols). The mode intensities for each spectrum are normalized against their respective G -mode strength. The multiphonon Raman signals from different nanotubes vary, but on the average are much stronger than the corresponding peaks for graphite.

The role of resonant Raman scattering also explains why a given multiphonon Raman mode in different nanotubes can exhibit significantly different strengths (Fig. 1): the excitonic transition energies in SWNTs depend sensitively on the precise chiral structure of the nanotube. The multiphonon Raman spectrum reflects correspondingly the electronic signature of the specific SWNT. We note that this sensitivity of the multiphonon Raman process to the nanotube electronic structure, which is clear in probing individual nanotubes, will be obscured in ensemble measurements of nanotubes of differing chiral structure. We can estimate the enhancement of a multiphonon Raman mode arising from resonance with an exciton transition by comparing the spectra of different nanotubes or the same nanotube excited by different laser wavelengths. We find an average resonant enhancement of ~ 20 at the peak of an exciton transition. Such an enhancement is consistent with a simple theoretical estimate using a typical linewidth of 80 meV for SWNT exciton transitions in the visible spectral range.

In summary, we have observed multiphonon Raman scattering from individual SWNTs involving up to 6 phonons. The strong and well-defined multiphonon lines are attributed to the combination of a significant electron-phonon coupling and near-resonant intermediate states in the Raman process. The features of Raman scattering of different modes and of the same mode in different nanotubes reflect the properties of the 1D excitonic transitions in SWNTs, as well as of the phonons themselves. Study of the polarization dependence and fine structure of the multiphonon Raman spectra should provide further detailed information on the electronic and phonon structure of the SWNTs.

The authors thank Dr. M. S. Dresselhaus, Dr. A. Jorio, Dr. J. Maultzsch, and Dr. V. Perebeinos for helpful dis-

cussions. We acknowledge support from the Office of Basic Energy Sciences, Materials Sciences and Engineering Division of the U.S. Department of Energy under Contract No. DE-AC03-76SF00098 (Berkeley researchers); from the Nanoscale Science and Engineering Initiative of the NSF under Grants No. CHE-0117752 and No. ECS-05-07111, the New York State Office of Science, Technology, and Academic Research (NYSTAR), and the Office of Basic Energy Sciences, U.S. Department of Energy (Grants No. DE-FG02-98ER-14861 and No. DE-FG02-03ER15463 (Columbia researchers). F. W. is grateful for the support from the Miller Institute of the University of California.

- [1] A. P. Alivisatos *et al.*, *J. Chem. Phys.* **90**, 3463 (1989).
- [2] M. C. Klein *et al.*, *Phys. Rev. B* **42**, 11 123 (1990).
- [3] T. D. Krauss, F. W. Wise, and D. B. Tanner, *Phys. Rev. Lett.* **76**, 1376 (1996).
- [4] R. Saito, G. Dresselhaus, and M. S. Dresselhaus, *Physical Properties of Carbon Nanotubes* (Imperial College Press, London, 1998).
- [5] A. M. Rao *et al.*, *Science* **275**, 187 (1997).
- [6] Z. H. Yu and L. E. Brus, *J. Phys. Chem. B* **105**, 6831 (2001).
- [7] C. Fantini *et al.*, *Phys. Rev. Lett.* **93**, 147406 (2004).
- [8] C. Thomsen *et al.*, *Phys. Status Solidi B* **242**, 1802 (2005).
- [9] R. Saito *et al.*, *New J. Phys.* **5**, 157 (2003).
- [10] J. E. Zucker *et al.*, *Phys. Rev. Lett.* **53**, 1280 (1984).
- [11] B. Jusserand and M. Cardona, in *Light Scattering in Solids V*, edited by M. Cardona and G. Guntherodt (Springer, Berlin, 1989), Vol. 66.
- [12] J. F. Scott, R. C. C. Leite, and T. C. Damen, *Phys. Rev.* **188**, 1285 (1969).
- [13] M. V. Klein and S. P. S. Porto, *Phys. Rev. Lett.* **22**, 782 (1969).
- [14] R. M. Martin and C. M. Varma, *Phys. Rev. Lett.* **26**, 1241 (1971).
- [15] R. Rodriguez-Suarez *et al.*, *Phys. Rev. B* **62**, 11 006 (2000).
- [16] L. M. Huang *et al.*, *J. Phys. Chem. B* **108**, 16 451 (2004).
- [17] M. Y. Sfeir *et al.*, *Science* **306**, 1540 (2004).
- [18] M. Y. Sfeir *et al.*, *Science* **312**, 554 (2006).
- [19] A. Jorio *et al.*, *Phys. Rev. Lett.* **86**, 1118 (2001).
- [20] M. S. Dresselhaus *et al.*, *Accounts Chem. Res.* **35**, 1070 (2002).
- [21] Y. Kawashima and G. Katagiri, *Phys. Rev. B* **52**, 10 053 (1995).
- [22] P. Tan *et al.*, *Appl. Phys. Lett.* **75**, 1524 (1999).
- [23] V. W. Brar *et al.*, *Phys. Rev. B* **66**, 155418 (2002).
- [24] B. A. Weinstein and M. Cardona, *Phys. Rev. B* **7**, 2545 (1973).
- [25] P. Y. Yu and M. Cardona, *Fundamentals of Semiconductors* (Springer, Berlin, 2004).
- [26] F. Wang *et al.*, *Science* **308**, 838 (2005).
- [27] J. Maultzsch *et al.*, *Phys. Rev. B* **72**, 241402 (2005).
- [28] V. Perebeinos, J. Tersoff, and P. Avouris, *Phys. Rev. Lett.* **92**, 257402 (2004).
- [29] C. D. Spataru *et al.*, *Phys. Rev. Lett.* **92**, 077402 (2004).